Non-normal global modes of supersonic jet noise

Joseph W. Nichols*[1] and Sanjiva K. Lele[1,2]

[1] Center for Turbulence Research, Stanford University
Stanford, CA 94305 USA
[2] Dept. of Aeronautics & Astronautics and Dept. of Mech. Engr., Stanford University
Stanford, CA, 94305 USA
* Corresponding author: jwn@stanford.edu

Global mode decomposition is applied to high speed jets over a range of jet-to-ambient density ratios and Mach numbers. Maximal transient response was obtained for each system by computing an optimal superposition of non-normal global modes. The non-normality of the global modes increased with decreasing density ratio as well as decreasing Mach number.

1 Introduction

The motivation for this research stems from the need to develop noise reduction strategies for aircraft engine exhausts. Sound levels in excess of 150 dB are consistently measured for a variety of high-performance tactical aircraft [17]. This poses a significant hazard for aircraft carrier ground and maintenance crews, as such an acoustic environment is beyond the capabilities of advanced hearing protection technology to prevent permanent hearing loss. Exhaust noise reduction is also a priority to the design of next generation supersonic civil transport to comply with international regulations regarding community noise.

Locally parallel [13] and weakly non-parallel [23] instability wave theories have met with moderate success at predicting noise generation in high-speed jets [5]. For supersonic jets, the mechanism of Mach wave radiation [22] provides a direct link between supersonically convecting instability waves and the acoustic far-field. Enhanced accuracy at minimal computational cost is obtained through the application of the linear [12] or nonlinear [1] parabolized stability equations (PSE). The PSE methodology, however, cannot capture upstream propagating waves, and breaks down in cases associated with strong heating [2].

The source of sound from transonic and subsonic jets remains less clear, because the convection velocity of instability waves in these cases is not sufficient to radiate sound directly. Nevertheless, recent studies [18, 21] show that energy can be transferred into the radiative part of the spectrum through nonlinear interaction of two instability waves. Wu and Huerre [25] show that nonlinear interaction of counterwinding helical modes of close frequency produces a slowly breathing mean-field distortion of azimuthal wavenumber $m = 2$ which efficiently radiates sound. In addition to nonlinear mode interactions, we propose the non-normality of the underlying linearized system as an alternate source of jet noise. In particular, we suggest the ϵ-pseudospectrum may extend into the radiative portion of spectral space even though the individual eigenmodes do not. Additionally, through the Kreiss matrix theorem, transient growth leads to an interpretation of jet noise without the need for harmonic forcing.

In this paper, global mode analysis is used as a tool to study the non-normality of the linearized system operator. While more computationally intensive, global mode analysis captures both the

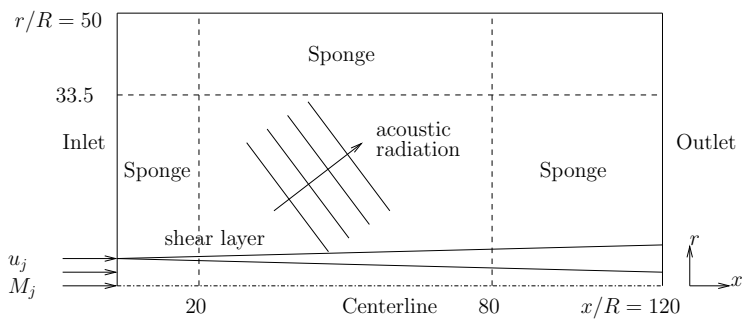

Figure 1: A schematic of the flow configuration.

effects of fully non-parallel base flows, as well as resolves upstream propagating waves. To observe the effects of jet-to-ambient density ratio (such as that produced by heating) as well as Mach number, we apply this method to a range of different base flows for which these parameters are varied systematically.

2 Flow configuration

Fig. 1 shows a cross-sectional schematic of sound production from a round, high-speed jet. The cylindrical coordinates x, r, and θ denote the axial, radial and azimuthal directions, respectively. The base flow, corresponding to a steady laminar jet, is assumed to be axisymmetric with respect to the centerline of the domain, shown at bottom. The jet enters the computational domain from the left and forms a shear layer as it encounters quiescent fluid within the domain. For a supersonic jet, hydrodynamic instability waves supported by the shear layer may couple directly with the acoustic modes radiating to the far field. To absorb outgoing acoustic waves and avoid reflections, numerical sponge layers are utilized at the streamwise and lateral boundaries.

The fully compressible Navier–Stokes equations are used as a mathematical model describing the dynamics of the supersonic jet. Similar to that of Sesterhenn [20], we use a pressure-velocity-entropy formulation, denoted as p, $\boldsymbol{u}$, and s, respectively.

$$\begin{aligned}
\frac{\partial p}{\partial t} &+ \boldsymbol{u}\cdot\nabla p + \rho c^2 \nabla\cdot\boldsymbol{u} = \frac{1}{M^2 Re Pr}\nabla^2 T, \\
\frac{\partial \boldsymbol{u}}{\partial t} &+ \frac{1}{\rho}\nabla p + \boldsymbol{u}\cdot\nabla\boldsymbol{u} = \frac{1}{Re}\frac{1}{\rho}\nabla\cdot\boldsymbol{\tau}, \\
\frac{\partial s}{\partial t} &+ \boldsymbol{u}\cdot\nabla s = \frac{1}{Re}\frac{1}{\rho T}\left(\frac{1}{(\gamma-1)M^2 Pr}\nabla^2 T + \Phi\right).
\end{aligned} \tag{1}$$

The equation of state for an ideal gas, $\gamma M^2 p = \rho T$, relates the fluid density ρ and temperature T to the pressure. The local speed of sound is defined as $c = \sqrt{\gamma p/\rho}$. $\boldsymbol{\tau}$ and Φ respectively represent the viscous stress tensor and dissipation, defined with $\mu_B/\mu = 0.6$, μ_B denoting the bulk viscosity. Assumed constant, $\gamma = 1.4$ is the ratio of specific heats. The jet Reynolds number is defined as $Re = \rho_j u_j R/\mu$ where ρ_j and u_j are the fluid density and velocity at the nozzle exit, R is the nozzle radius, and μ is the dynamic viscosity, assumed constant. The Prandtl number is defined as $Pr = c_p\mu/\lambda$, where c_p is the specific heat at constant pressure and λ is the thermal conductivity. For all calculations in this paper, $Re = 3600$ and $Pr = 1$. The jet Mach number is defined as $M^2 = u_j^2/\bar{c}_j^2$ where $\bar{c}_j$ is the speed of sound at the nozzle exit conditions.

Steady base flows are obtained by solving the compressible boundary layer equations together with the Crocco-Busemann relation [11], about which the system is linearized. The linearized Navier–Stokes (LNS) equations are discretized by fourth-order centered finite differences applied

M_j	M_a	S	
1.5	1.25	1.45	supersonic, cold
1.5	1.5	1.0	supersonic, isothermal
1.5	2.12	0.5	supersonic, hot
2.5	1.67	2.25	strongly supersonic, cold
0.9	0.83	1.16	transonic, cold

Table 1: The five flow configurations considered in this study, differing by jet Mach number M_j and density ratio S. The resulting acoustic Mach number M_a is also given.

on a stretched but structured mesh to yield a large sparse matrix. Global modes of the system were then extracted using a shift-and-invert Arnoldi method as implemented by the software package ARPACK [9]. The inversion step was computed by finding the LU decomposition of the shifted sparse matrix using the massively parallel SuperLU package [10]. Code verification was accomplished by comparison with published results [12]. Further details about the implementation and verification of the code considered in this study can be found in [15, 16].

3 Results

This section presents results of similar calculations performed on a series of five different jet base flows. As summarized in table 1, these jets differed in two parameters: the jet Mach number M_j and the jet-to-ambient density ratio S. The acoustic Mach number, defined as $M_a = u_j/c_\infty$ where c_∞ is the ambient speed of sound, is determined by M_j and S. As a base case, we consider a cold supersonic jet with $M_j = 1.5$ and $S = 1.45$. This density ratio corresponds to a condition where the stagnation temperature of the jet is equal to the ambient temperature. The next two cases with the same jet Mach number, study the effect of heating with respect to the base case, by incrementally decreasing the density ratio. The final two cases aim to capture effects of Mach number compared to the base case, while maintaining the cold condition.

3.1 Effect of density ratio

Fig. 2 compares spectra of global eigenfrequencies obtained for the $M = 1.5$ jet at three different density ratios. Each of the spectra contains an arching branch over low frequencies, that we will see is associated with Kelvin–Helmholtz instability. We will refer to it as the branch of type (a) global modes. At higher frequency, each spectrum also contains a kinked branch of type (b) global modes. These modes can be shown [15] to be associated with the subsonic family of modes predicted by Tam and Hu [24]. As the density ratio decreases, the position of the entire spectrum shifts upwards and to the left, corresponding to less damping and lower frequencies. In the cases of $S = 1.45$ and $S = 1.0$, all of the eigenvalues lie below the real axis indicating global instability, whereas for $S = 0.5$, some eigenvalues have crossed above the axis into the unstable half-plane. Note that this happens for type (a) modes only, whereas type (b) modes remain stable.

Fig. 3 shows global modes corresponding to the labeled arrows of fig. 2. The left-hand column shows the least-damped type (a) mode arising from K–H instability, while the right-hand column shows the leading type (b) modes corresponding to the subsonic modes of [24]. For the type (a) modes, the angle of the Mach-wave radiation is observed to increase with decreasing density ratio S. This can be explained by noting that the speed of sound exterior to the jet decreases relative to the speed of sound inside the jet as the jet is heated, so that the acoustic Mach number $M_a = u_j/c_\infty$ increases with heating. The effect of heating is more pronounced for type (b) global modes. For $S = 1.45$, the mode upstream of the onset of the outlet sponge is primarily composed of an upstream propagating wave. As heating increases, a downstream propagating wave component becomes increasingly evident. Because a global mode must have zero group velocity, in fact all of

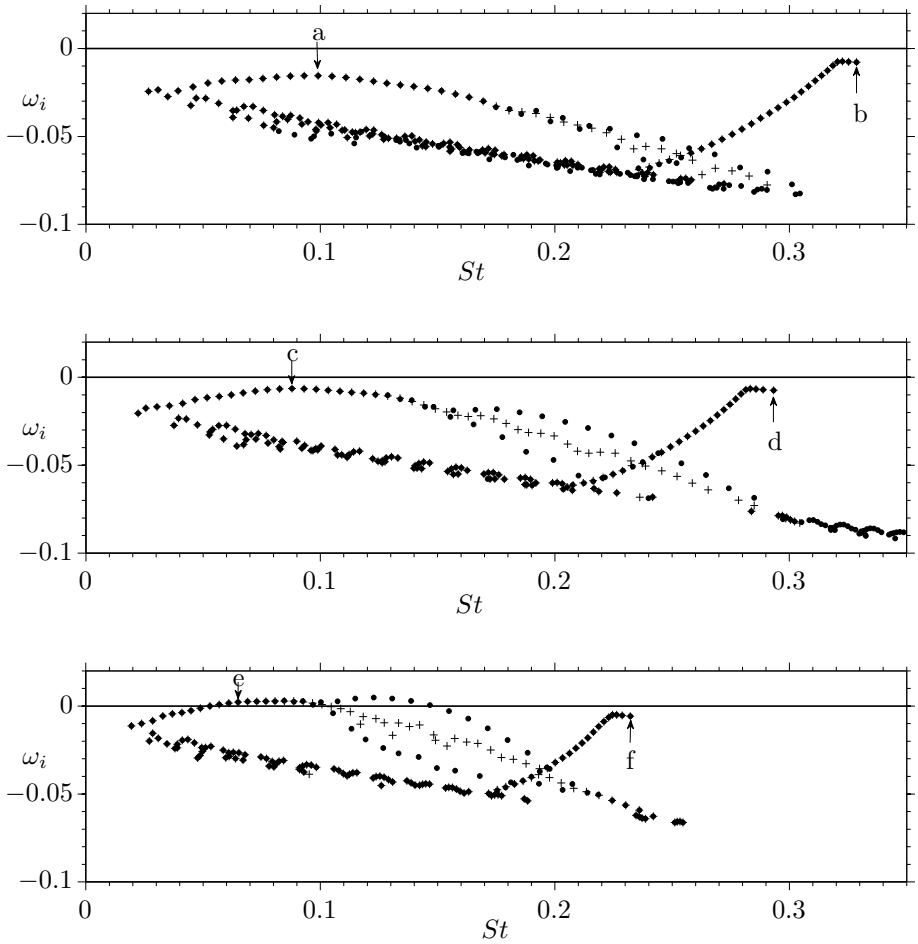

Figure 2: From top to bottom, spectra of global eigenfrequencies for the cold, isothermal, and hot $M = 1.5$ jets. Direct (•) and negative conjugate adjoint (+) eigenfrequencies are shown.

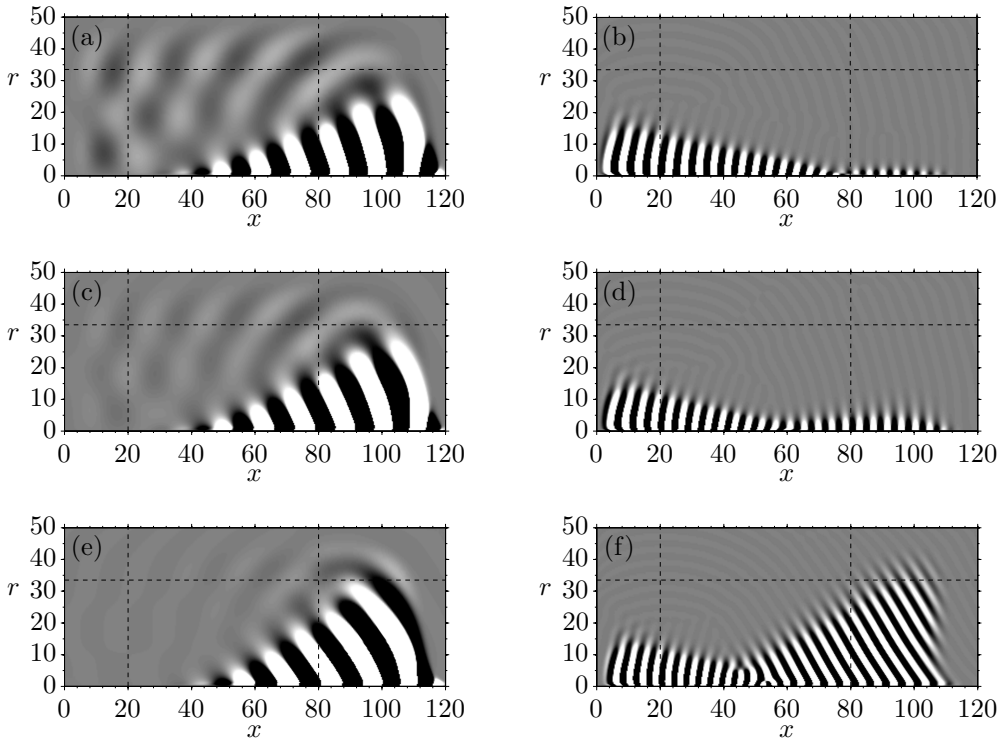

Figure 3: Global modes corresponding to the labels of fig. 2, visualized by contours of the real part of the perturbation pressure.

modes displayed in figure 3 should have both an upstream propagating wave component as well as a downstream propagating wave component, but the relative strengths of these components may vary.

In each spectrum shown in fig. 2, the branch of type (a) modes splits near its right hand edge. This split becomes more pronounced with decreasing density ratio S, and in the case of $S = 0.5$, leads to the most unstable eigenfrequencies of the system. We observe, however, that the agreement between the direct ($\bullet$) and the conjugated adjoint ($+$) eigenvalues breaks down in the region of the split, indicating that this behavior owes to numerical rather than physical causes. Because the adjoint eigenvalues were computed using a continuous adjoint approach [14], there is no intrinsic numerical reason that they should be negative conjugate to the direct eigenvalues, unless both the direct and adjoint discretizations provide adequate models of the underlying continuous problems. In fact, the close agreement of the direct and adjoint eigenvalues over most of the spectra shown in fig. 2 indicates a high level of convergence for the corresponding modes. In addition, this method enables us to detect that this convergence breaks down near to the split, whereas a discrete adjoint approach may miss this fact.

To ascertain the source of the breakdown in convergence in the vicinity of the split, we consider the ϵ-pseudospectrum associated with the hot supersonic jet ($S = 0.5$). A complex value z is defined to be an ϵ-pseudo-eigenvalue of the system matrix A if the resolvent norm $||(zI - A)^{-1}||$ is greater than or equal to $1/\epsilon$. For normal matrices, the resolvent norm is simply the inverse of the minimum distance between z and and eigenvalue of A. For non-normal systems, however, the resolvent can also be large for z values far away from eigenvalues through a phenomenon known as pseudo-resonance. While an approximation for the pseudo-spectrum can be computed in the basis of extracted global modes, an adjoint solver allows us to compute the exact resolvent norm in the entire system space. We apply the power method to determine the largest eigenvalue of

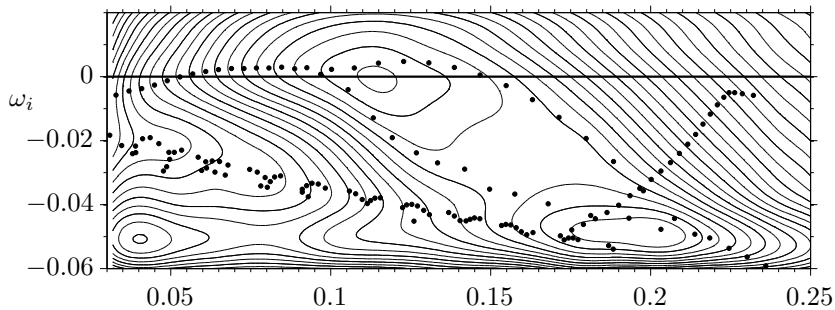

Figure 4: Contours of the resolvent norm for the hot $M = 1.5$ jet.

$(z^*I - A^*)^{-1}(zI - A)^{-1}$, corresponding to the square of the resolvent norm. Note that the shift-and-invert steps of this method are the exactly the same as those employed by the Arnoldi method to extract global modes. In addition, we obtain the optimal forcing function (mapping to maximal output) for frequency z as the eigenvector corresponding to this largest eigenvalue.

Fig. 4 shows the resulting contours of the resolvent norm for the hot jet. For clarity, a logarithmic scale has been used for the contour levels. We observe that the resolvent norm reaches a maximum in the region of the split, and that the shape of the split spectrum agrees somewhat with the shape of the contours of the resolvent norm in this region. An alternate, equivalent definition of the ϵ-pseudospectrum is that it is the set of points corresponding to eigenvalues of $A + E$ for all random matrices E with $||E|| < \epsilon$. Therefore, the contours within the split spectrum indicate the level of numerical precision of the method, both inherent to the discretization, and that demanded by the stopping criterion of the Arnoldi method. For convectively non-normal systems, [7] observe that a lack of numerical precision gives rise to similar hoop-shaped spectra. As the numerical precision increased, these hoop-shaped spectra were observed to behave like zip-fasteners, converging upon straight lines. For our jets, we find that the maximum level of the resolvent norm of the cold $M = 1.5$ jet (not shown) is less than than the maximum level of the hot $M = 1.5$ jet, indicating a greater level of non-normality in the case of the hot jet. This explains the greater prominence of the split spectrum as S decreases, and is consistent with the spatial structure of the type (a) global modes observed in fig. 3.

3.2 Effect of Mach number

Fig. 5 shows global spectra resulting from the cold $M = 0.9$ and $M = 2.5$ jets. The spectrum for the $M = 0.9$ jet contains a large branch of type (a) global modes, some of which may be slightly unstable. This branch shows a large split, however, suggestive of strong non-normality, which we will later confirm. Fig. 6(a) visualizes a representative global mode taken from the low frequency portion of the branch, ahead of the split.

In contrast, the spectrum of the $M = 2.5$ jet appears to contain two branches of type (b) global modes, while the branch of type (a) global modes is mysteriously missing. The two branches of type (b) modes correspond to the first and second subsonic modes of [24], and as figs. 6(c) and (d) show, can be distinguished by the number of radial zero crossings in the jet core. In fact, the type (a) branch is not absent, but has all but merged with the cloud of damped eigenvalues corresponding to standing acoustic modes of the rectangular domain. The location of this branch may be recovered by considering which modes contribute most to the optimal superposition computed in the next section. These modes are highlighted by circles in fig. 5(b) and a corresponding mode shape is shown in fig. 6(b).

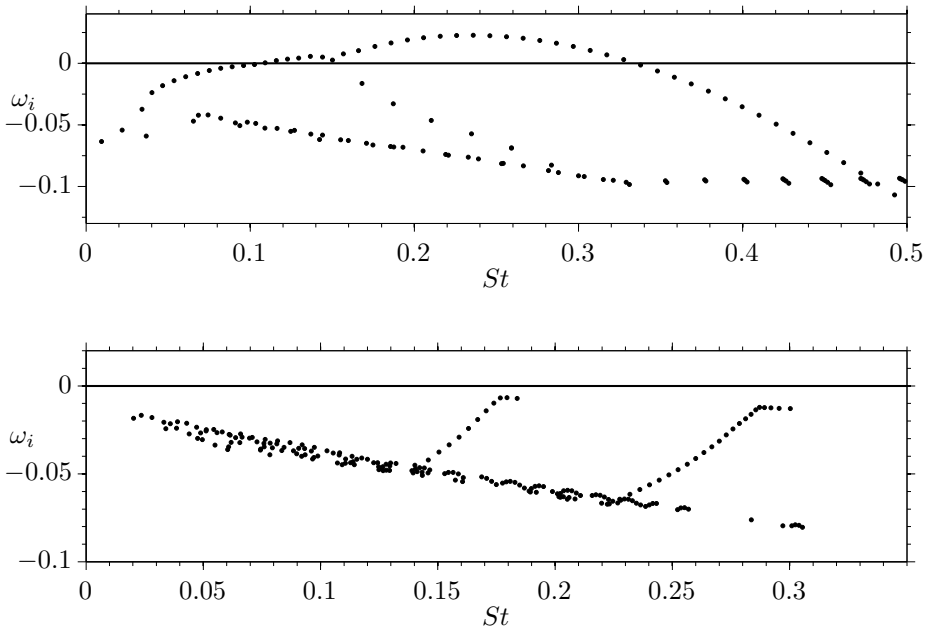

Figure 5: Spectra of global eigenfrequencies for the cold (a) $M = 0.9$ and (b) $M = 2.5$ jet.

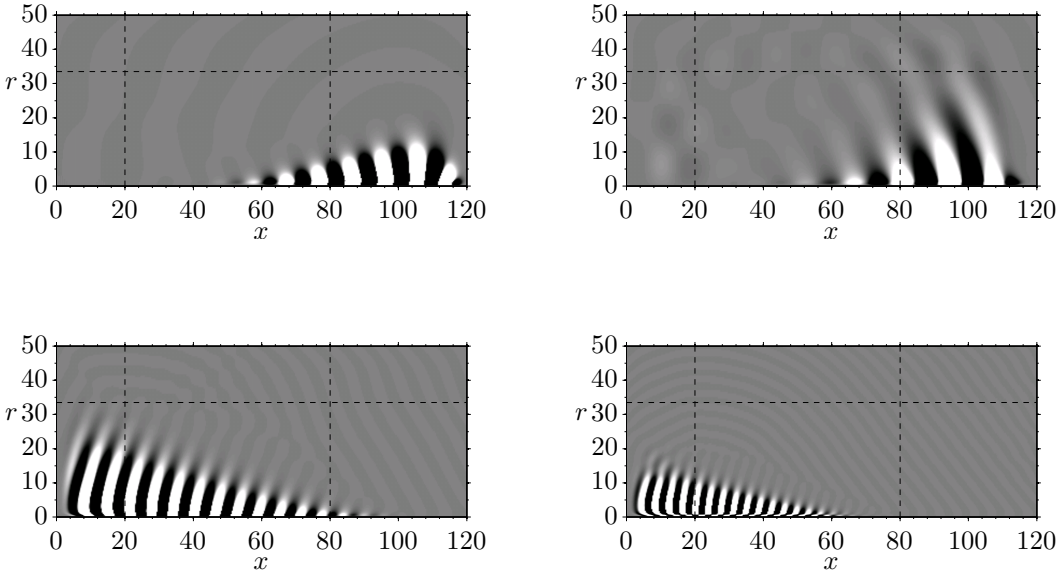

Figure 6: Global modes corresponding to the labels of fig. 5, visualized by contours of the real part of the perturbation pressure.

3.3 Non-normal transient response

The majority of global modes presented above were found to be temporally damped. In the two cases of globally unstable jets, the few amplifying modes at best predict weak growth for the long-time behavior of the system. At finite times, however, a large transient growth is possible through the superposition of these non-normal global modes. Indeed, as we have seen previously, the resolvent norm remains large (exceeding even the numerical range provided by double precision floating point arithmetic) over a significant portion of the ϵ-pseudospectrum, indicating strong non-normal effects. In this section, we quantify the non-normality of each jet by finding the computing the superposition of corresponding global modes that leads to maximal transient growth. The optimal superposition is found by singular value decomposition, following [19]. In this analysis, the transient growth is measured in terms of the disturbance energy, defined for a compressible flow as:

$$E = \int\int \left[\frac{\bar{\rho} u_i u_i^*}{2} + \frac{M^2 |p|^2}{2} + \frac{\gamma(\gamma-1) M^2 |s|^2}{2} \right] r dr dx, \tag{2}$$

where * signifies the complex conjugate. This norm was shown to be positive definite and monotone non-increasing for quiescent compressible fluids by [3], and independently derived by [6] by eliminating conservative compression work transfer terms. With respect to this norm, we define the maximum amplification G of the disturbance energy as:

$$G(t) = \max \frac{||\boldsymbol{q}(t)||_E^2}{||\boldsymbol{q}(0)||_E^2}, \tag{3}$$

where $\boldsymbol{q}(0)$ and $\boldsymbol{q}(t)$ represent the system state at the start and end of the time interval considered, respectively. It is important to note that this amplification depends on the duration t of the finite interval considered, so that the curve $G(t)$ represents an envelope of all possible transient responses.

While the disturbance energy seems a natural choice of norm, there are certainly other viable choices, and we may expect them to lead to different results. For an example from aeroacoustics, the far-field overall sound pressure level (OASPL) of the radiative acoustic waves, perhaps with frequency-weighting to account for human perception, is another such norm of interest. The reader is cautioned, however, that the norm used for the denominator of 3 must be full with respect to all state variables. On the other, hand employing different norms for the numerator and denominator is an intriguing possibility which has been explored recently by [8]. Clearly, the choice of norm warrants further investigation for this problem, but this remains beyond the scope of this paper.

Fig. 7 shows the curves $G(t)$ for each of the five jets considered. The bold solid line represents our base case of the cold $M = 1.5$ jet. We find that the amplification reaches a maximum of $G = 3.885 \times 10^9$ for a time interval $t \approx 129$. The thin dashed and dot-dashed lines represent the isothermal and hot $M = 1.5$ jets, respectively, and we observe that heating significantly increases the transient growth. This is consistent with the observation that heating increases the streamwise separation between the direct and adjoint global modes, and as such increases the convective non-normality of the system. For the hot $M = 1.5$ jet, the transient growth was found to reach a maximum level of $G = 5.8909 \times 10^{14}$ for $t = 188$. Fig. 7 also shows $G(t)$ for the $M = 2.5$ and $M = 0.9$ cold jets, represented by the bold dashed and dot-dashed curves, respectively. Comparing these curves to that of the cold $M = 1.5$ jet, it is evident that the non-normality increases with decreasing Mach number. For the $M = 0.9$ jet, the transient growth reaches $G = 6.268 \times 10^{16}$ for $t = 140$, which is the maximum obtained for all five cases.

To understand the nature of this transient growth, fig. 8 visualizes the development of the system state q from the optimal initial condition is visualized in figure 8. The five rows of frames correspond to the five different jets considered, and each contains a time series of three images corresponding to $t = 0, 50, 100$ from left-to-right. Note that each sequence is taken along a trajectory leading to maximum transient growth for each case, but the time intervals have been kept constant between successive frames for fair comparison. In each sequence, a wavepacket is initiated near the nozzle and then grows as it propagates through the domain. Clearly, the global modes, which do not resemble much a wavepacket, nevertheless provide an adequate basis in each case to capture this

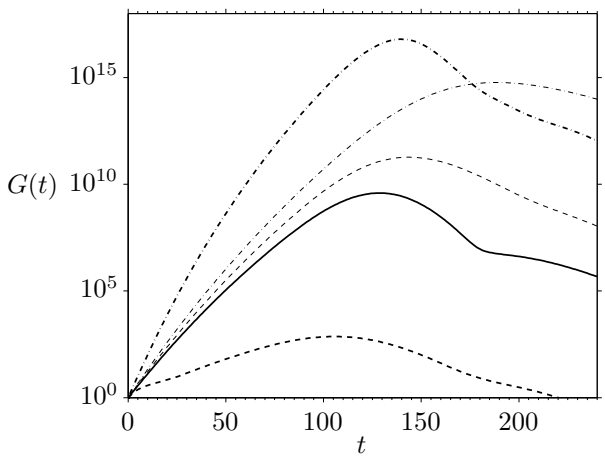

Figure 7: Transient growth envelopes $G(t)$ for the cold, $M = 1.5$ ——— ; isothermal, $M = 1.5$ ---- ; hot, $M = 1.5$ —·— ; cold, $M = 2.5$ ---- ; and cold $M = 0.9$ —·— jets.

type of convective instability, in agreement with the theory developed by [4].

Comparing the first three rows of fig. 8, we observe that the convection speed of the wavepacket decreases as heating increases. In fig. 7, note also that the amplification curves peak for at increasingly late times as heating increases, consistent with a wavepackets that propagate more slowly through the domain. We also note that the angle of the emitted sound increases with increasing heating, which can be explained as before as an effect of the increasing acoustic Mach number. We therefore interpret the effect of heating as a shift of the wavepacket peak to lower group velocities, in analogy to locally parallel stability theory. Also, this shifting may eventually cause the upstream edge of the wavepacket to be able to withstand the oncoming flow, causing the flow to become globally unstable.

The last two rows of fig. 8 compare the transient response of cold $M = 2.5$ and $M = 0.9$ jets, respectively. The acoustic waves associated with the $M = 2.5$ jet, radiate at a clear angle, consistent with Mach wave emission. In contrast, there is no such angle associated with response of the $M = 0.9$ jet. The transient response of the cold $M = 1.5$ jet shown in the first row of fig. 8 is somewhere between these two extremes. While the angle of the acoustic disturbances appears to vary throughout the wavepacket of the $M = 0.9$ jet, the wavepacket is seen to develop a elongated upstream tail (lower right-most frame) in which the angle approximately equilibrates. If this pattern continues to an unbounded setting, this tail might be interpreted as acoustic radiation at low angles to the jet axis. Recall that the transient growth predicted for the $M = 0.9$ jet was the strongest of all the jets, and as such non-normality may play an important role in acoustic production in transonic jets where the acoustic Mach number is too low for the Mach wave emission to be active.

4 Conclusions

All of the jets considered in this study, ranging from strongly supersonic to transonic and from cold to hot, were found to exhibit significant non-normality. In each case, the optimal superposition of global modes resulted in a propagating and growing wavepacket, showing the convective nature of this non-normality. We observed that the character of the wavepacket could be modified through modification of the density ratio and Mach number. Lower density ratios, corresponding to increased heating, led to increased non-normality and larger transient growth. The peak of the wavepacket was observed to shift to lower group velocities with increased heating, so the increased

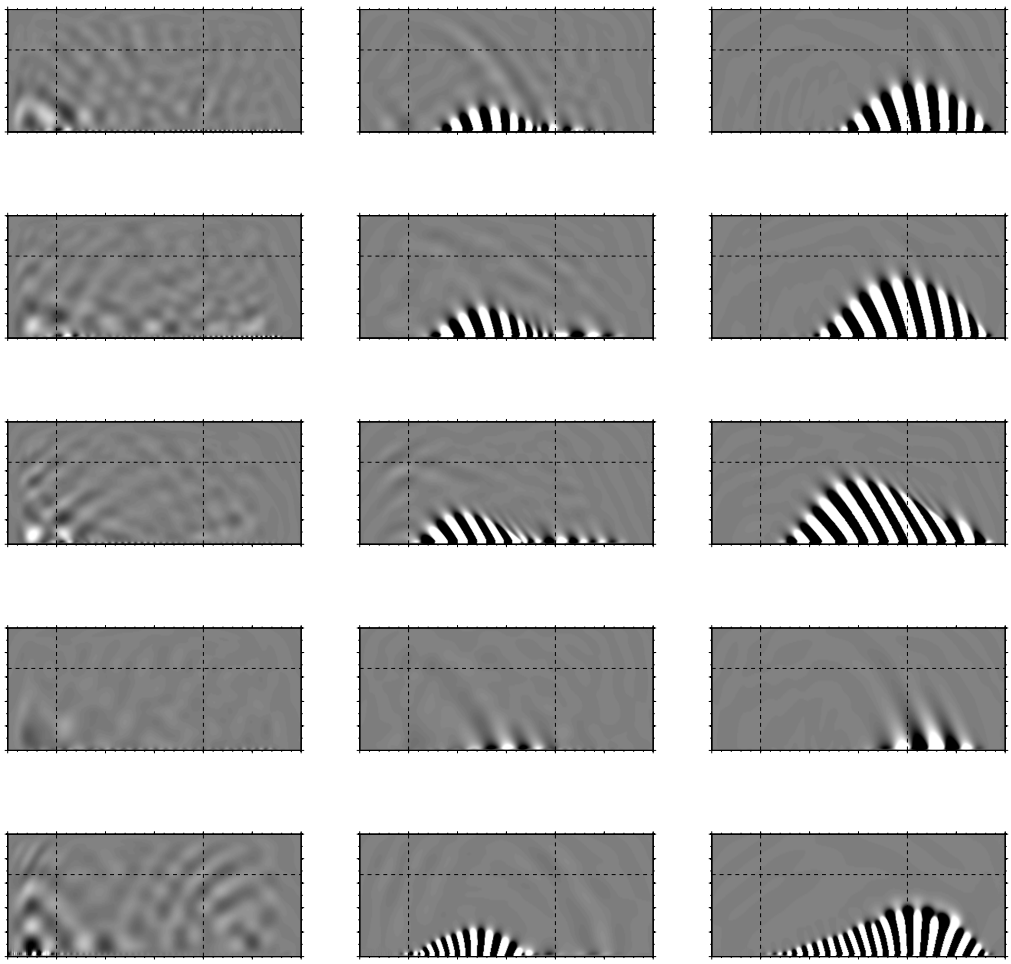

Figure 8: Time sequences of the optimal transient response for the five different jets considered. The top three rows correspond to the cold, isothermal, and hot $M = 1.5$ jets, respectively, followed by the cold $M = 2.5$ jet and finally the cold $M = 0.9$ jet. In each sequence, the columns correspond to the times $t = 0, 50, 100$ from left to right.

growth may partially owe to the wavepacket having a longer time interval over which to grow. The jet Mach number had an even greater effect on non-normality than density ratio, and we found the non-normality to increase significantly as the Mach number decreased. For the $M = 0.9$ cold jet, we found a maximum transient energy amplification of more than 16 orders of magnitude. The wavepacket associated with this case differed somewhat from the wavepackets observed in the supersonic cases. For the supersonic jets, a primary angle of acoustic radiation was observed, associated with the acoustic Mach number in each case. While no one such angle was discernible over the entire wavepacket in the case of the transonic jet, a long upstream tail was observed to form in which this angle remained relatively constant and as such might be interpreted as "non-normal" acoustic radiation.

References

[1] L. C. Cheung, D. J. Bodony, and S. K. Lele. Noise radiation predictions from jet instability waves using a hybrid nonlinear pse-acoustic analogy approach. In *Proceedings of the 13th AIAA/CEAS Aeroacoustics Conference (28th AIAA Aeroacoustics Conference)*, 2007.

[2] Lawrence C. Cheung and Sanjiva K. Lele. The dynamics of nonlinear instability waves in laminar heated and unheated compressible mixing layers. *Physics of Fluids*, 21:094103, 2009.

[3] B.-T. Chu. On the energy transfer to small disturbances in fluid flow (part i). *Acta Mechanica*, 1:215–234, September 1965.

[4] C. Cossu and J.-M. Chomaz. Global measures of local convective instabilities. *Phys. Rev. Lett.*, 78:4387–4390, 1997.

[5] D. G. Crighton. Orderly structure as a source of jet exhaust noise: Survey lecture. In *Structure and mechanisms of turbulence II*, volume 76 of *Lecture Notes in Physics*, page 154–170, Berlin/Heidelberg, 1978. Springer.

[6] A. Hanifi, P. J. Schmid, and D. S. Henningson. Transient growth in compressible boundary layer flow. *Physics of Fluids*, 8:826, 1996.

[7] C. J. Heaton, J. W. Nichols, and P. J. Schmid. Global linear stability of the non-parallel batchelor vortex. *Journal of Fluid Mechanics*, 629:139–160, 2009.

[8] J. Jiménez. Localized amplification of energy in turbulent channels. *Annual Research Briefs, Center for Turbulence Research*, pages 423–433, 2009.

[9] R. B. Lehoucq, D. C. Sorensen, and C. Yang. *ARPACK Users' Guide: Solution of Large-Scale Eigenvalue Problems with Implicitly Restarted Arnoldi Methods*. SIAM, 1998.

[10] X. S. Li and J. W. Demmel. SuperLU_DIST: A scalable distributed-memory sparse direct solver for unsymmetric linear systems. *ACM Trans. Mathematical Software*, 29(2):110–140, June 2003.

[11] G. Lu and S. K. Lele. A numerical investigation of skewed mixing layers. Technical Report TF-67, Dept. of Mech. Eng., Stanford University, 1996.

[12] M. Malik and C.-L. Chang. Nonparallel and nonlinear stability of supersonic jet flow. *Computers & Fluids*, 29:327–365, March 2000.

[13] A. Michalke. Survey on jet instability theory. *Progress in Aerospace Sciences*, 21:159–199, 1984.

[14] S. Nadarajah and A. Jameson. A comparison of the continuous and discrete adjoint approach to automatic aerodynamic optimization. *AIAA paper*, (AIAA-2000-0667), 2000.

[15] J. W. Nichols and S. K. Lele. Global modes and transient response of a cold supersonic jet. *Journal of Fluid Mechanics*, (submitted), 2010.

[16] J. W. Nichols, S. K. Lele, and P. Moin. Global mode decomposition of supersonic jet noise. *Annual Research Briefs, Center for Turbulence Research*, pages 3–15, 2009.

[17] NRAC. *Naval Research Advisory Committee Report on Jet Engine Noise Reduction*, April 2009.

[18] Neil D Sandham, C. L. Morfey, and Z. W. Hu. Nonlinear mechanisms of sound generation in a perturbed parallel jet flow. *Journal of Fluid Mechanics*, 565:1, September 2006.

[19] P. J. Schmid and D. S. Henningson. *Stability and Transition in Shear Flows*. Springer-Verlag, New York, 2001.

[20] J. Sesterhenn. A characteristic-type formulation of the Navier–Stokes equations for high order upwind schemes. *Computers & Fluids*, 30(1):37–67, 2000.

[21] V. Suponitsky and N. D. Sandham. Nonlinear mechanisms of sound radiation in a subsonic jet. In *Proceedings of the 15th AIAA/CEAS Aeroacoustics Conference (30th AIAA Aeroacoustics Conference)*, pages 1–21, Miami, 2009.

[22] C. K. W. Tam. Supersonic jet noise. *Annual Review of Fluid Mechanics*, 27:17–43, January 1995.

[23] C. K. W. Tam and D. E. Burton. Sound generated by instability waves of supersonic flows. part 2. axisymmetric jets. *Journal of Fluid Mechanics*, 138:273, April 1984.

[24] C. K. W. Tam and F. Q. Hu. On the three families of instability waves of high-speed jets. *Journal of Fluid Mechanics*, 201:447–483, 1989.

[25] X. Wu and P. Huerre. Low-frequency sound radiated by a nonlinearly modulated wavepacket of helical modes on a subsonic circular jet. *Journal of Fluid Mechanics*, 637:173, September 2009.